ChemPubSoc Europe

DOI: 10.1002/chem.201801523

CHEMISTRY A European Journal Full Paper

Magnetic Properties

Exchange Interactions Switch Tunneling: A Comparative Experimental and Theoretical Study on Relaxation Dynamics by Targeted Metal Ion Replacement

Haiquan Tian,*[a, b] Liviu Ungur,*[c] Lang Zhao,[a] Shuai Ding,[d] Jinkui Tang,*[a] and Liviu F. Chibotaru[c]

Dedicated to Professor Dai-Zheng Liao on the occasion of his 80th birthday

Abstract: The magnetic relaxation and magnetization blocking barriers of tailor-made homo- and heterodinuclear compounds $[Dy_2(opch)_2(OAc)_2(H_2O)_2]\cdot MeOH$ (**1**) and $[DyMn(opch)_2(OAc)(MeOH)(H_2O)_2]$ (**2**), where H_2opch is (*E*)-*N*′-(2-hydroxy-3-methoxybenzylidene)pyrazine-2-carbohydrazide, were systematically investigated and the change in single-molecule magnet behavior originating from targeted replacement of one dysprosium site in the Dy_2 compound with manganese was elucidated through a combination of experimental and theoretical studies. A detailed comparative study on these closely related model compounds revealed remarkable changes of the crystal-field splitting and anisotropy of the Dy site and the total exchange spectrum due to the replacement of Dy by Mn. The blocking barriers of these two compounds, which explain their different relaxation behaviors, were analyzed. The two Ising doublets arising from the magnetic interaction in the case of **1** are strongly uniaxial, with tunneling splittings smaller than 10^{-6} cm^{-1}, and this leads to magnetic relaxation at temperatures exceeding the exchange energy (2.14 cm^{-1}), which involves transition via the excited states corresponding to local transitions on the excited doublet at the Dy site. The third and fourth exchange doublets in **2** (located at 2.16 and 3.25 cm^{-1}, respectively) show much larger tunneling splittings (of 10^{-4} and 10^{-3} cm^{-1}, respectively), and thus open an important path for magnetic relaxation.

Introduction

Single-molecular magnets (SMMs) that exhibit magnetic bistability of purely molecular origin approach the ultimate size limit for spin-based devices, and this has made them almost ideal candidates in high-density data storage technologies and molecular spintronics since their discovery in the early 1990s.[1] The requisite for such a system is an energy barrier to reversal of the magnetization *U*, which is derived from a combination of an appreciable spin ground-state *S* and magnetoanisotropy *D*.[2] Apparently, the success of such technological applications hinges on raising the blocking temperature T_B and inherent anisotropic barriers *U*.

Throughout the development of SMMs,[3] transition metals have acted as pioneers during a relatively long period with several remarkable results, such as magnetic hysteresis of 4.5 K and magnetization reversal of 84.6 K in a $[Mn_6]$ compound.[4] In particular, a two-coordinate cobalt imido compound based on the highly covalent Co=N core achieved a highly effective energy barrier to magnetization reversal of 594 K and exhibited magnetic blocking below 9.5 K.[5] By contrast, lanthanide SMMs have developed at an extraordinary pace since the discovery in 2003 that a mononuclear Tb^{III} compound shows slow relaxation of the magnetization.[6] Accompanied by the establishment of the most important landmark, the threshold spin-relaxation barrier of 1000 K has been crossed by several outstanding monometallic compounds in the last two years, including a few Dy complexes, namely, [Dy(bbpen)Br],[7] $[Dy(O^tBu)_2(py)_5][BPh_4]$,[8] and $[(Cp^{ttt})_2Dy][B(C_6F_5)_4]$[9]. The last one is the champion of the energy barrier and the magnetic hysteresis temperature with values of 1837 and 60 K, respectively. Modulating the hyperfine interactions in a non-Kramers Ho^{III} single-

[a] Dr. H. Tian, Dr. L. Zhao, Prof. Dr. J. Tang
State Key Laboratory of Rare Earth Resource Utilization
Changchun Institute of Applied Chemistry
Chinese Academy of Sciences
Changchun 130022 (P. R. China)
E-mail: tang@ciac.ac.cn

[b] Dr. H. Tian
Shandong Provincial Key Laboratory
of Chemical Energy Storage and Novel Cell Technology
School of Chemistry and Chemical Engineering
Liaocheng University, Liaocheng 252000 (P. R. China)
E-mail: tianhaiquan@lcu.edu.cn

[c] Dr. L. Ungur, Prof. Dr. L. F. Chibotaru
Department of Chemistry, KU Leuven
Celestijnenlaan 200F, 3001 Leuven (Belgium)
E-mail: Liviu.Ungur@kuleuven.be

[d] S. Ding
Shandong Juye County Coal Board
Juye 274900 (P.R. China)

Supporting information and the ORCID identification number(s) for the author(s) of this article can be found under:
https://doi.org/10.1002/chem.201801523.

ion magnet (SIM) allowed the fast quantum tunneling of the magnetization (QTM) at zero field to be suppressed and a high energy barrier (341 K) to be achieved.[10] Another striking finding is that the exceptionally strong magnetic exchange brought about by the diffuse spin of an N_2^{3-} radical bridge in dinuclear compounds hinders the QTM and thus affords a record blocking temperature of 14 K.[11]

The Dy_2 complexes have indisputably played a key role in elucidating the relaxation mechanism.[12] Retrospectively, by virtue of the diamagnetic Y_2 matrix, the magnetic dilution method was employed to elucidate the influence of the neighboring Dy^{III} ion in a single-ion relaxation mechanism based on a centrosymmetric dinuclear Dy_2 compound.[12b] The blocking mechanism principally originates from the individual Dy^{III} sites, and the exchange interaction between the sites in an asymmetric Dy_2 SMM was revealed by taking advantage of a combination of experimental and high-level ab initio calculations.[12c] On the other hand, utilization of the stronger magnetic exchange between transition metal and lanthanide ions is a promising route to integrate large magnetic anisotropies and high-spin ground states, mainly because the synthesis of 3d–4f heterosystems is relatively simple compared to that of radical-containing systems. Heterometallic $[M_2Ln_2]$ ($M = Co^{II}$, Cr^{III}, Ru^{III}; $Ln = Gd^{III}$, Tb^{III}, Dy^{III}) model systems were explored in which different transition metal ions were embedded in lanthanide systems to elucidate the relaxation mechanism and to enhance the blocking temperature.[13] Although the effects of different trivalent 3d ions on the relaxation dynamics have been unambiguously identified in the above-mentioned $[M_2Ln_2]$ system, the targeted replacement of lanthanide with 3d ions in an elegant dinuclear lanthanide model to probe the effects that 3d ions (replacing 4f ions) have on the relaxation dynamics has not been explored. A comparative investigation into such homo- and heterodinuclear models will provide insight into the influence that the 3d ions have on the system and how they affect the static and dynamic magnetic behavior.

We therefore selected the versatile (*E*)-*N*′-(2-hydroxy-3-methoxybenzylidene)pyrazine-2-carbohydrazide (H_2opch) hydrazone ligand in order to assemble the aforementioned two model complexes. In our previous studies, the H_2opch ligand has been successfully applied to construct four polynuclear Dy^{III}-based SMMs thanks to its flexible coordination modes under different reaction conditions, as depicted in Scheme 1.

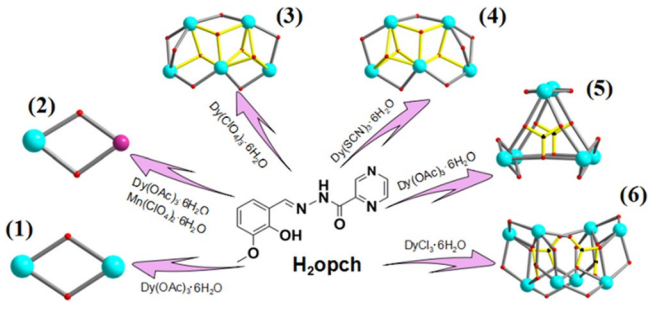

Scheme 1. Six SMMs originating from the H_2opch proligand and different Dy^{III} salts.

Compounds **3** and **6** exhibit butterfly-shaped topologies with peculiar mirror images of each other, and the latter has a larger anisotropic energy gap of 197 K and a longer characteristic relaxation time τ of 3.5 s.[14] Additionally doubly and quadruply CO_3^{2-} bridged dinuclear Dy^{III} cores have been obtained (compounds **5** and **4**) by spontaneous fixation of two and four atmospheric CO_2 molecules, respectively.[15]

Herein we report the isolation of homo- and heterodinuclear $[Dy_2(opch)_2(OAc)_2(H_2O)_2]\cdot MeOH$ (**1**) and $[DyMn(opch)_2(OAc)(MeOH)(H_2O)_2]$ (**2**). These two structurally closely related model complexes provide a unique opportunity to probe simultaneously the contributions of 3d and 4f ions as well as their exchange interaction on the relaxation dynamics. Ab initio calculations were applied to get insight into the influence that the individual 3d and 4f ions and their interaction have on the system and how they affect the static and dynamic magnetic behavior. Besides, detailed experimental characterization of structure and magnetism, a thorough description of the local electronic and magnetic properties of Dy sites, including the calculated crystal field parameters, is given. In addition, the obtained results were correlated with the calculated charges on neighboring ligand atoms, and the exchange interaction and the exchange spectrum were subsequently described. Through such a detailed comparative study, we were able to compare the changes in structure, magnetic properties, and crystal-field splitting and anisotropy of the Dy site, the total exchange spectrum, and exchange parameters due to the replacement of Dy with Mn. Finally, the blocking barriers in these two compounds, which explain their different blocking behaviors, were analyzed.

Results and Discussion

Structural analysis of H_2opch

The multidentate Schiff-base H_2opch ligand was obtained by reaction of pyrazine-2-carbohydrazide and *o*-vanillin aldehyde. This ligand provides N,O,N,O,O-based multichelating sites that are especially favorable for the formation of lanthanide compounds. The molecular structure of H_2opch determined by single-crystal X-ray diffraction is depicted in Figure S1 and the crystal data are summarized in Table S1 (Supporting Information). The ligand crystallizes in the monoclinic space group *C*2/*c* with eight molecules in each unit cell. The free ligand is planar and in the keto form, as the C(9)–O(3) distance of 1.214 (5) Å corresponds to a carbon–oxygen double bond. The adjacent molecules are linked by intermolecular hydrogen bonds N2–H2···N4$^{\#1}$, C13–H13···N3$^{\#1}$, and C1–H1C···O1$^{\#2}$ (symmetry codes: #1, 1.5−*x*, 0.5+*y*, 1.5−*z*; #2, 2.5−*x*, 0.5−*y*, 1−*z*), generating a two-dimensional supramolecular plane, as shown in Figure S2 of the Supporting Information.

Structural analysis of 1

The reaction of $Dy(OAc)_3\cdot 6H_2O$ with H_2opch (1:1 ratio) in $MeOH/CH_2Cl_2$ (1:1 ratio) in the presence of triethylamine (3 equiv) produced golden yellow crystals of

$[Dy_2(opch)_2(OAc)_2(H_2O)_2]\cdot MeOH$ (**1**) in 46% yield in one week. The molecular structure determined by single-crystal X-ray diffraction is depicted in Figure 1. Compound **1** crystallizes in the triclinic space group $P\bar{1}$ with $Z=1$. Details of the structure solution and refinement are summarized in Table S1 (Supporting Information), and selected bond lengths and angles are listed in Table 1 and Table S2 of the Supporting Information. The molecular structure of this compound exhibits a center of symmetry with a Dy···Dy distance of 3.891(1) Å and two Dy-O-Dy angles of 113.1(2)°. Two $opch^{2-}$ hydrazone ligands behave as a pair of tetradentate N_2O_2 ligands to coordinate two Dy^{III} centers, whereby the two Dy^{III} ions are doubly bridged by the carboxyl oxygen atoms (O_3 and O_{3a}) with Dy–O distances of 2.324(1) and 2.338(1) Å. Each of the Dy^{III} centers is further coordinated by one acetate anion in a bidentate fashion, as well as by one terminal water molecule to complete the N_2O_6 environment based on a distorted dodecahedral geometry (Figure 1, top). A closer look at the crystal structure of **1** reveals that coordination of two water molecules and two acetate groups to Dy1 and Dy1a above and below the $opch^{2-}$–Dy^{III} plane produces a hula hoop-like coordination geometry, which is believed to be crucial for the observation of SMM behavior in related Dy_2 compounds.[12c] The Dy–O bond lengths are in the range of 2.145(1)–2.419(1) Å and the two Dy–N bond lengths are 2.478(2) and 2.565(2) Å. Only one $2.1_1 1_1 2_{12} 2_2$ coordination mode (Harris notation)[16] can be observed for the H_2opch ligand in its doubly deprotonated form (Scheme S1 in the Supporting Information). Additionally one noncoordinated methanol molecule is located in the crystal lattice. Finally, strong inter- and intramolecular hydrogen-bonding interactions produce a two-dimensional supramolecular plane with the **acs** net (4,4),[17] as shown in Figure S3 of the Supporting Information. The shortest intermolecular Dy···Dy distance is 8.563(1) Å.

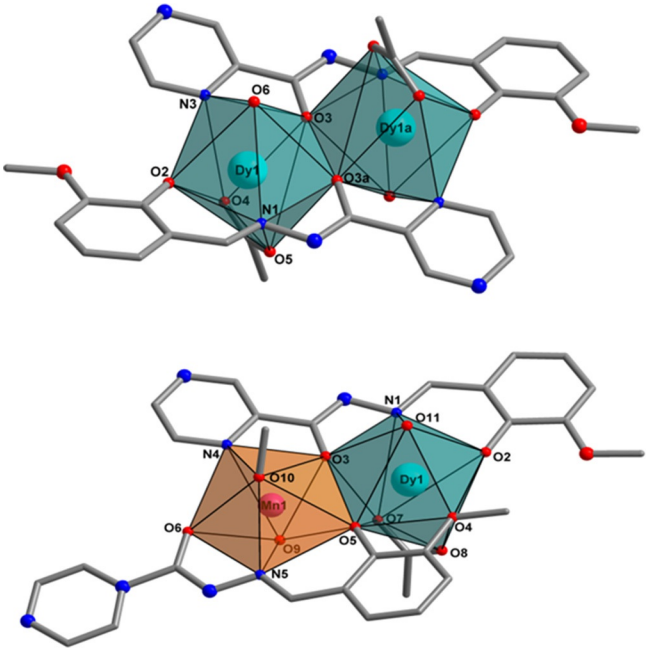

Figure 1. Molecular structures of **1** (top) and **2** (bottom). Hydrogen atoms and lattice solvent are omitted for clarity. Color scheme: turquoise Dy, dark rose Mn, red O, blue N.

Table 1. Selected bond lengths [Å] and angles [°] for **1** and **2**.

Compound **1**			
Dy1–O3	2.324(1)	Dy1–O3a	2.338(1)
Dy1–O4	2.419(1)	Dy1–N3	2.566(2)
Dy1–O5	2.363(1)	Dy1–N1a	2.478(2)
Dy1–O6	2.362(1)	Dy1···Dy1a	3.891(2)
Dy1–O2a	2.145(1)	Dy1-O3-Dy1a	113.1(2)
Compound **2**			
Mn1–O3	2.188(1)	Mn1–O10	2.079(1)
Mn1–O5	2.314(1)	Mn1–N4	2.422(1)
Mn1–O6	2.313(1)	Mn1–N5	2.354(2)
Mn1–O9	2.242(1)	Mn1···Dy1	3.727(2)
Mn1-O3-Dy1	112.5(1)	Mn1-O5-Dy1	106.6(1)

Structural analysis of 2

The reaction of $Dy(OAc)_3\cdot 6H_2O$, $Mn(ClO_4)_2\cdot 6H_2O$, and a solution of H_2opch in $MeOH/CH_2Cl_2$ (1:1 v/v) in the presence of triethylamine (3 equiv) led to the formation of a dinuclear heterometallic DyMn compound after three weeks, namely, $[DyMn(opch)_2(OAc)(MeOH)(H_2O)_2]$ (**2**). Single-crystal X-ray diffraction revealed that **2** crystallizes in the monoclinic space group $P2_1/c$ with $Z=4$. A perspective view of the molecular structure of **2** is shown in Figure 1, the crystal data are summarized in Table S1 (Supporting Information), and selected bond lengths and angles are listed in Table 1 and Table S2 (Supporting Information). In the asymmetric molecule, two $opch^{2-}$ polydentate Schiff-base ligands provide N,O,N,O- and O,N,O,O-based multichelating sites to chelate Mn^{II} and Dy^{III}. In so doing, two metal centers are doubly bridged by the phenol oxygen atom (O_3) and the carboxyl oxygen atom (O_5) with a Mn···Dy distance of 3.726(1) Å and two Mn-O-Dy angles of 112.5(1) and 106.6(1)°. Completion of the coordination sphere of Mn1 by water and methanol molecules generates an N_2O_5 environment with nearly perfect pentagonal-bipyramidal coordination geometry, whereas the Dy1 ion adopts a distorted dodecahedral geometry based on an NO_7 environment, which resembles that of the Dy^{III} ions of compound **1** (Figure 1, bottom). Here, two H_2opch ligands show $2.1_1 1_1 2_{12} 2_2$ and $2.1_1 2_{12} 1_2 3_2$ coordination modes in the doubly deprotonated form (Scheme S1 in the Supporting Information), with the latter observed for the first time for this ligand. Meanwhile, this is the first example of the opch ligand coordinating to 3d metal ions. The Mn–O bond lengths are in the range of 2.01(1)–2.318(1) Å, and the two Mn–N bond lengths are 2.358(2) and 2.425(2) Å, respectively. The Dy–O bond lengths are in the range of 2.174(1)–2.469(1) Å and only one Dy–N bond length is 2.458(2) Å. Strong intermolecular hydrogen-bonding interactions produce a one-dimensional zigzag chain of molecules (Figure S4 in the Supporting Information). The shortest intermolecular Mn···Dy distance is 6.901(1) Å.

Comparison of the molecular structures of 1 and 2

The Dy_2 core of compound **1** and the DyMn core of compound **2** are embedded in the same ligands with the following main differences: Firstly, only one kind of N_2O_6 environment can be found in compound **1** with only one binding mode of the two opch ligands, while an N_2O_5 environment of the Mn^{II} ion and eightfold coordination of the Dy^{III} ion are present in compound **2**, derived from two binding modes of the ligands. The magnetic properties of SMMs are influenced not only by the coordination environments of the metal ions, but also by other subtle effects induced by their nearest neighbors. Furthermore, for lanthanide SMMs, the geometry of the core is strongly correlated to the nature or directions of the easy axes of anisotropic ions. According to this peculiarity, the SHAPE software was used to quantify the geometry of the coordination center cations.[18] A systematic analysis of the resulting parameters (Table S3 in the Supporting Information) revealed that an intermediate geometry between triangular dodecahedron (D_{2d}) and square antiprism (D_{4d}) can be observed for the octacoordinate Dy^{III} ions of compounds **1** and **2**. The heptacoordinate Mn^{II} ion shows a nearly pentagonal-bipyramid (D_{5h}) geometry with a shape measure deviation of 0.647. On the other hand, we observed that the Dy···Mn distance (3.728(1) Å) in compound **2** is much shorter than the Dy···Dy distance (3.891(1) Å) in compound **1**, and the short intermolecular distance is strongly affected, with values of 8.563(1) and 6.901(1) Å for compounds **1** and **2**, respectively.

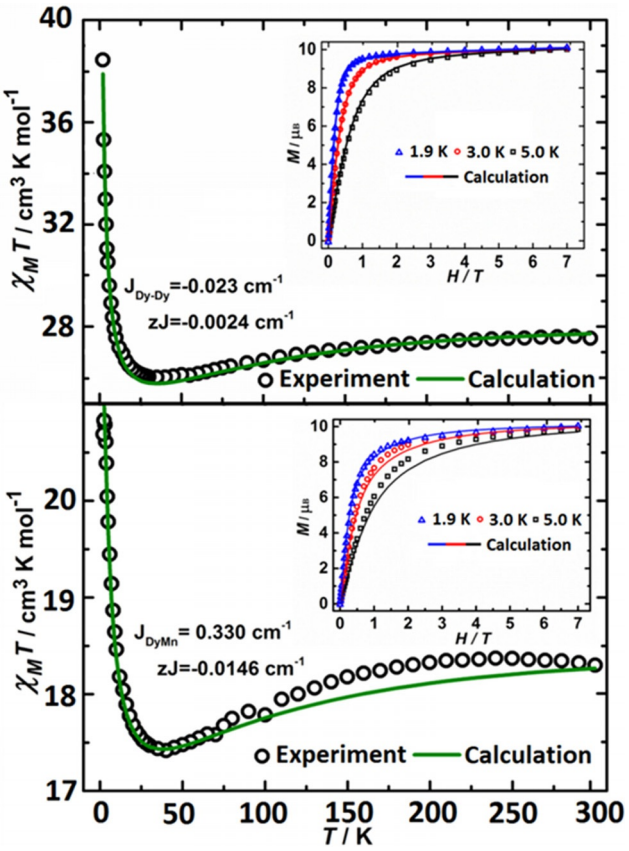

Figure 2. Temperature dependence of $\chi_M T$ at 1000 Oe for **1** (top) and **2** (bottom). Inset: *M* versus *H*/*T* plots at different temperatures below 5 K.

Magnetic properties

Static susceptibility measurements on polycrystalline samples of compounds **1** and **2** were carried out in the temperature range 2–300 K in an applied field of 1000 Oe. The plots of $\chi_M T$ versus *T*, where χ_M is the molar magnetic susceptibility, are shown in Figure 2. The $\chi_M T$ value of 28.1 $cm^3 K mol^{-1}$ for compound **1** at room temperature is in good agreement with the expected value of 28.34 $cm^3 K mol^{-1}$ for two uncoupled Dy^{III} ions ($S=5/2$, $L=5$, $^6H_{15/2}$, $C=14.17$ $cm^3 K mol^{-1}$ with $g=4/3$). The $\chi_M T$ value decreases slightly to a minimum value of 27.4 $cm^3 K mol^{-1}$ with decreasing temperature, which is mainly ascribed to the progressive depopulation of excited Stark sublevels.[2f,m,19] With further decreasing temperature, the $\chi_M T$ value then increases sharply to a maximum of 38.4 $cm^3 K mol^{-1}$ at 2 K, which obviously suggests the presence of intramolecular ferromagnetic interactions between the metal centers, as observed in other Dy^{III} compounds.[20] For compound **2**, the $\chi_M T$ value of 15.6 $cm^3 K mol^{-1}$ at 300 K is lower than the theoretical value of 18.55 $cm^3 K mol^{-1}$ (Mn^{II}: $S=5/2$, $C=4.375$ $cm^3 K mol^{-1}$ with $g=2$; and Dy^{III}: $S=5/2$, $L=5$, $^6H_{15/2}$, $C=14.17$ $cm^3 K mol^{-1}$ with $g=4/3$). The $\chi_M T$ product gradually decreases with decreasing temperature and reaches a minimum value of 17.4 $cm^3 K mol^{-1}$ at 40 K, which is a typical decrease, induced by depopulation of excited Stark sublevels of the Dy^{III} ions.[21] The $\chi_M T$ value exhibits a sharp increase below 20 K (maximum of 20.8 $cm^3 K mol^{-1}$ at 2 K), indicating the presence of intramolecular ferromagnetic interactions between the metal centers.[2n,o,22] Clearly, the disparity of the two curves is most likely due to the difference of the overall magnetic interaction between metal centers in these compounds.

The magnetizations of the two complexes from zero dc field to 70 kOe at different temperatures are shown in the inset of Figure 2, with maximum values at 1.9 K of 10.1 (**1**) and 10.0 μ_B (**2**), where μ_B is the Bohr magneton. These values are lower than the expected saturation values of 20 (**1**) and 15 μ_B (**2**) for two noninteracting Dy^{III} ions ($g_J \times J = {}^4/_3 \times {}^{15}/_2 = 10$ μ_B per Dy^{III} ion) and one isolated Mn^{II} (5 μ_B per Mn^{II} ion with $S=5/2$ and $g=2$) and one Dy^{III} ion, respectively. This is most likely due to significant anisotropy and the crystal-field effect in the system for **1** and **2**.[3c] At low fields, the magnetization in **1** increases more rapidly than that of **2**. Meanwhile, the nonsuperposition of the *M* versus *H*/*T* data on a single master curve and the high-field nonsaturation suggests the presence of significant magnetic anisotropy and/or low-lying excited states in **1** and **2**.[23] To further characterize the dynamics of magnetization, a series of ac susceptibility measurements at different frequencies and temperatures were carried out for compound **1** in zero dc field (Figure 3 and Figures S5 and S6 in the Supporting Information). The strong frequency dependence of both in-phase (χ') and out-of-phase (χ'') susceptibilities reveals the onset of slow relaxation of the magnetization that is typical of SMM behavior. The $\chi'T$ value exhibits a rapid decrease around 17 K for 1500 Hz, which is coincident with emerging peak of

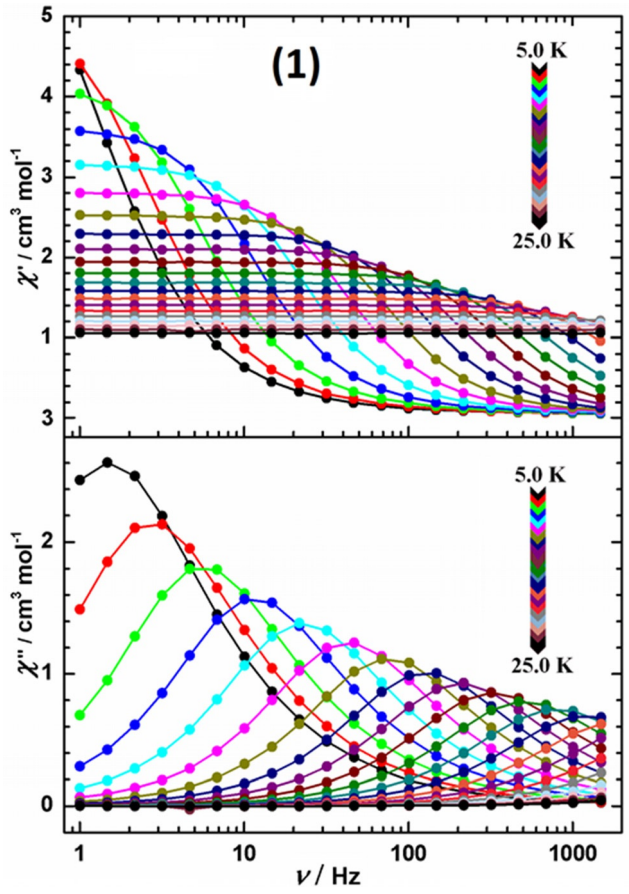

Figure 3. Frequency dependence of the in-phase (top) and out-of-phase (bottom) ac susceptibility of **1** in zero dc field.

the χ'' signal when the magnetization is blocked by the anisotropy barriers. The Cole–Cole plots of χ'' versus χ' were constructed and fitted to a generalized Debye model to obtain α values and relaxation times τ in the temperature range 3.0–19.0 K (Figure 5, top, inset).

This revealed a relatively narrow distribution of τ with small α parameters (0.008–0.17, Figure S7 in the Supporting Information).[11] From frequency dependencies of the ac susceptibility, the magnetization relaxation times were deduced in the temperature range of 1.9–17.0 K and the $\ln\tau$ versus T^{-1} plots obtained from these data are shown in Figure 5. At high temperature, the relaxation follows a thermally activated Orbach mechanism[24] with $\Delta = 95.2$ cm^{-1} and $\tau_0 = 4.2\times10^{-8}$ s based on an Arrhenius law [$\tau = \tau_0 \exp(\Delta/kT)$]. Below 3 K, there is a temperature-independent characteristic time of $\tau_{QTM} = 0.17$ s, as expected in a pure quantum relaxation regime.

For compound **2**, no obvious out-of-phase signals were observed above 1.9 K in zero dc field (Supporting Information, Figure S8), and this indicates very fast relaxation of the magnetization. To further investigate the relaxation behavior and look for quantum tunneling effects, the frequency-dependent ac susceptibility was measured with application of dc fields up to 2000 Oe at 1.9 K (see Figure S9 in the Supporting Information). Remarkably, application of a dc field has a strong influence on the dynamic behavior of their magnetization, which suggests the presence of fast QTM.[25] As seen in ac susceptibility signals, the relaxation mode is slightly moved to higher frequency with increasing field, and the Cole–Cole plot exhibits a series of evident asymmetric semicircles under variable static fields (between 600 and 2000 Oe), as depicted in Figure S10 of the Supporting Information. All the above features indicate that the applied field has an important effect on the relaxation process.[26]

To obtain quantitative information regarding the relaxation barrier of compound **2**, the frequency dependence of χ'' in 1000 Oe applied dc field was examined below 18.0 K, as shown in Figure 4 and Figures S11–S13 of the Supporting Information. This behavior indicates field-induced slow relaxation of the magnetization. The maximum values of the temperatures and frequencies are observed in the 1.9–8.0 K range. From these data, the Cole–Cole plots (Figure 5 bottom, inset) were constructed with a series of asymmetric semicircles; moreover, the generalized Debye model cannot fit these data well and gives a large α value of about 0.24 (see Figure S12 in the Supporting Information), which indicates a wide distribution of τ.[27] All the above features suggest the presence of multiple relaxation pathways. These distinctly larger α values compared to those of **1** may be due to the substitution of Dy^{III} by Mn^{II} and the slight changes in the ligand field caused by the replacement of an acetate ligand by a methanol ligand. To

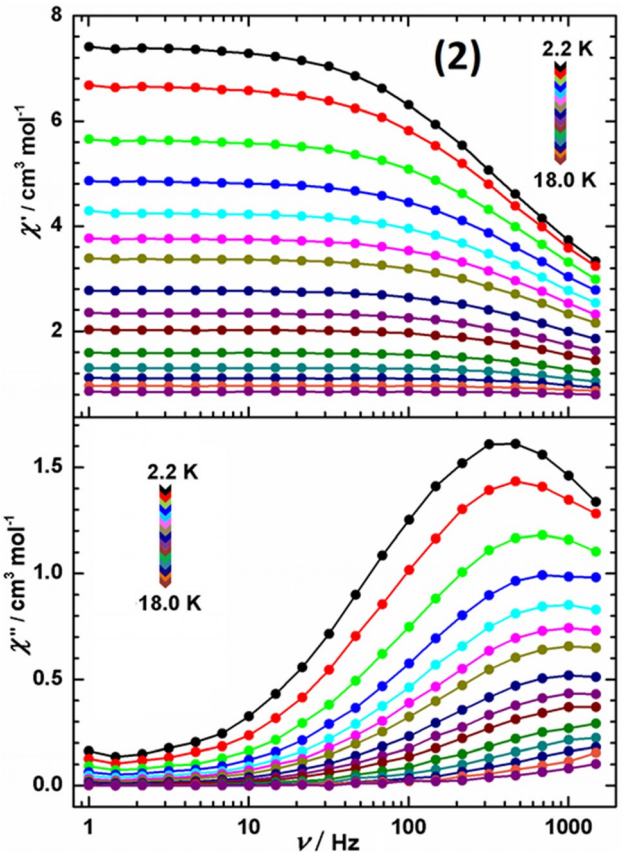

Figure 4. Frequency dependence of the in-phase (top) and out-of-phase ac susceptibility of compound **2** under a 1000 Oe dc field.

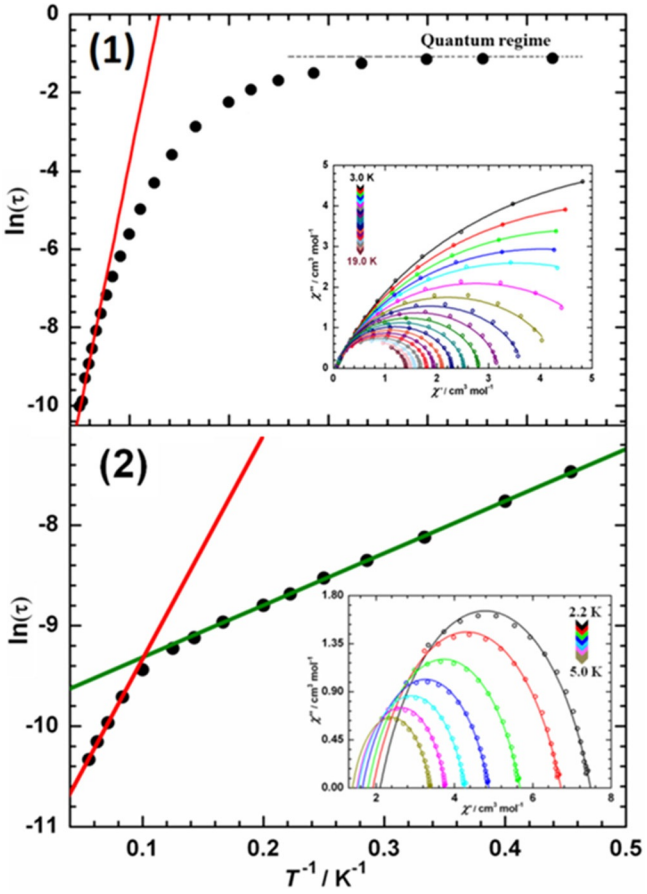

Figure 5. Magnetization relaxation time $\ln\tau$ versus T^{-1} at 0 Oe (**1**, top) and 1000 Oe (**2**, bottom) dc field. The solid line was fitted with the Arrhenius law (see text); inset: Cole–Cole plots. The solid lines are the best fits to the experimental data.

quantify the relaxation barrier, the relaxation time was then extracted from the frequency-dependent data between 2.2 and 18.0 K, and the Arrhenius plot obtained from these data is shown in Figure 5. Interestingly, two relaxation regimes are clearly visible with a transition between them corresponding to Δ of 3.7 and 36.2 cm^{-1} and τ_0 of 4.9×10^{-5} and 1.8×10^{-7} s for the low- and high-temperature domains, respectively. The observation of multiple relaxation processes is the result of the presence of the distinct anisotropic center of a single Dy^{III} ion and the exchange interaction between the Dy^{III} and Mn^{II} ions.[13a,b]

Comparison of magnetic properties of 1 and 2

The temperature dependence of the susceptibility for **1** and **2** shows similar intramolecular ferromagnetic interactions between the metal centers at temperatures below about 40 K, while the $\chi_M T$ product conspicuously decreases from 300 to 40 K in **2** and a slightly declining tendency is observed in the same temperature range for **1**. This variation of $\chi_M T$ at higher temperatures is directly correlated to the replacement of a Dy^{III} ion with an Mn^{II} ion. Regarding ac susceptibility, for **1**, a single process of slow relaxation of the magnetization can be detected, which gives a thermal energy barrier for the reversal of magnetization of 95.2 cm^{-1} without the external dc field. In contrast, **2** exhibits a complex behavior of the two-step relaxations by providing a small dc field. To interpret the origin of their magnetic properties, we performed ab initio theoretical calculations on **1** and **2**, a method that is very applicable for the investigation of lanthanide compounds.[2f,g,28]

Computational details

Fragment ab initio CASSCF calculations were performed on **1** and **2** with the MOLCAS program package.[29] Two basis set approximations were employed: 1) a medium-sized DZP-quality basis set and 2) a large TZP-quality basis set corresponding to the following contractions: for the DZP basis set: [7s6p4d2f1g] for Dy^{III} ions, [3s2p] for all N and C atoms, and [2s] for H atoms; for the TZP basis set: [8s7p5d4f2g1h] for Dy^{III} ions, [4s3p1d] for N and C atoms in the first and second coordination spheres, [3s2p] for distant C atoms, and [2s] for H atoms (see Table S2 in the Supporting Information). For Dy^{III}, the active space of the CASSCF method included the nine electrons from the last shell spanning seven 4f orbitals, CAS(9,7). All active molecular orbitals contain about 99.8% contribution from the 4f basis functions of the Dy site. State-average CASSCF calculations were performed for all possible spin states. All spin-sextet states (^{6}H, ^{6}F, and ^{6}P manifolds) and some of the spin-quartet states (128 out of 224) and spin-doublet states (130 out of 490) were further mixed by the spin–orbit interaction within the restricted active space state interaction (RASSI) method, resulting in a spin–orbital spectrum comprising 898 states, grouped in doublets (Kramers doublets, KD). On the basis of the resulting spin–orbit multiplets the SINGLE_ANISO program[30] computed local magnetic properties (*g* tensors, main magnetic axes, local magnetic susceptibility, parameters of the crystal field for the ground atomic multiplet, etc). Exchange spectra and magnetism of the binuclear compounds were simulated by using the POLY ANISO software[30] on the basis of the ab initio results. More details are given in the Experimental Section.

All broken-symmetry (BS)-DFT calculations were done with the ORCA program package[31] by using the B3LYP exchange correlation functional. All atoms were described by relativistic split-valence + polarization basis sets (SVP-DKH) or by large relativistic def2-triple-zeta valence + polarization basis (def2-TZVPP).[32] Relativistic corrections were accounted for in the Douglas–Kroll–Hess formalism, truncated at the second order (default implementation). The strictest convergence criteria for the self-consistent field energy minimization was employed (VeryTightSCF) in combination with the most accurate angular grids for the grid integration accuracy (Grid7).

Ab initio investigation of local electronic and magnetic properties of Dy sites in 1 and 2

Ab initio calculations on the individual Dy^{III} magnetic sites were performed to find the local electronic structure and magnetic anisotropy. Table 2 and Tables S5 and S6 (Supporting Information) show the obtained spectrum of the low-lying KDs

Table 2. Energies [cm^{-1}] and g tensors of the low-lying Kramers doublets (KD) of Dy sites in **1** and **2** obtained in the largest computational model employed.

KD		Dy in Dy_2 (**1**)		Dy in DyMn (**2**)	
		E	*g*	*E*	*g*
	g_x		0.00656		0.00377
1	g_y	0.000	0.01297	0.000	0.00746
	g_z		19.47883		19.60838
	g_x		0.20683		0.09764
2	g_y	191.727	0.24975	204.075	0.14829
	g_z		16.64449		16.68307
	g_x		1.73682		2.43880
3	g_y	333.817	3.00333	365.896	4.01876
	g_z		15.63005		15.24130
	g_x		1.66865		8.30491
4	g_y	353.559	5.31728	423.700	5.18753
	g_z		11.80336		1.34074
	g_x		1.44494		8.37729
5	g_y	415.434	3.80855	537.958	6.74977
	g_z		12.14542		2.28868
	g_x		1.19377		1.92027
6	g_y	442.544	2.07300	585.852	3.15284
	g_z		16.24514		15.15655
	g_x		0.44372		0.30107
7	g_y	513.722	1.15980	671.784	0.52062
	g_z		15.03593		17.15311
	g_x		0.23857		0.12276
8	g_y	579.318	0.53052	754.154	0.14069
	g_z		18.07661		19.33366

arising from the crystal-field splitting of the free-ion $J=15/2$ manifold of the Dy^{III} ion and their magnetic anisotropy. We note the large energy separation between the ground and first excited doublet, of about 190–200 cm^{-1}, as well as the strong uniaxial magnetic anisotropy of the ground doublet states ($g_{x,y} \ll g_z$; see Figure S14 in the Supporting Information). The main magnetic axis (g_z) of the ground doublets on the dysprosium sites form a small angle with the shortest Dy–O2 chemical bonds (dashed lines in Figure 6) and lie approximately in the plane formed by the two bridging oxygen atom and two dysprosium ions. The reasons for this orientation are the electrostatic and covalent effects arising from the O2 oxygen ligand atom, which apparently produces the strongest effect on the Dy site. The ab initio calculated LoProp atomic charges[33] on all atoms are listed in Tables S7 and S8 of the Supporting Information. Note that the O2 oxygen atom does not exert the largest electrostatic effect in both compounds. The angle between the main magnetic axes (g_z) of the ground and first excited Kramers doublets is larger in **1** than in **2** (20.4 and 8.6°, respectively; Tables S9 and S10 in the Supporting Information), which indicates a slighter larger contribution to tunneling in the first excited state. For both **1** and **2**, the calculated excitation energy between the ground and first excited state is higher than the value of a single thermally activated relaxation regime extracted from the ac susceptibility data (95.2 cm^{-1}). We can assume that in the high-temperature regime magnetic relaxation of the Dy_2 compound occurs by several relaxation processes, some of which have a lower activation barrier, which results in the effective activation barrier extracted from ac measurements [Figures 7 (top) and 8 (top)].

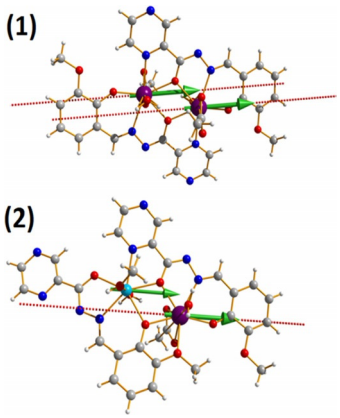

Figure 6. Calculated orientations of the local magnetic axes (dashed lines) and the magnetic moments in the ground exchange state (green arrows) on the metal sites in **1** and **2**.

Ab initio investigation of magnetic coupling in 1 and 2

To estimate the sign and magnitude of the exchange coupling in **1** and **2**, we performed BS-DFT calculations (as described above). On the other hand, exchange coupling was found from the fitting of experimental data with the POLY ANISO program. On the basis of calculated exchange spectrum, the temperature-dependent magnetic susceptibility (see Figure 2) and high-field magnetization at low temperatures (see Figure 2, inset) are described. Table 3 and Table S11 (Supporting Information) compare the extracted exchange coupling parameters in the investigated compounds.

In the case of **1**, both BS-DFT calculations and the fitting of the experimental data predict quite small antiferromagnetic exchange coupling (Table 3 and Table S12 in the Supporting Information). However, the total magnetic interaction between Dy sites in **1** is ferromagnetic due to the strong dipolar magnetic interaction between large moments on the Dy^{III} sites, which stabilizes their parallel arrangement (Figure 6). The latter, in turn, originates from a near-parallel alignment of the local anisotropy axes and the axis connecting the Dy^{III} ions.

In the case of **2**, exchange interaction is much stronger than the magnetic dipolar coupling, which is normal for a 4f–3d interaction. BS-DFT calculations also predict ferromagnetic coupling. Calculated energy spectra for both compounds are given in Table 4. We note that the two Ising doublets arising from the magnetic interaction in the case of **1** are strongly uniaxial with tunneling splittings smaller than 10^{-6} cm^{-1}. This explains why **1** shows blocking of the magnetization. Magnetic relaxation at temperatures exceeding the exchange energy (2.14 cm^{-1}) must involve transition via the excited states, which correspond in this case to local transitions at the excited doublet on the Dy site (Figure 7 bottom).

The low-lying exchange spectrum of **2** is formed by six Ising doublets (Figure 8), originating from the exchange interaction of the ground doublet on Dy and the $S=5/2$ on Mn (Table 4). Here the third and fourth exchange doublets in **2** (located at 1.94 and 2.91 cm^{-1}, respectively) show much larger tunneling

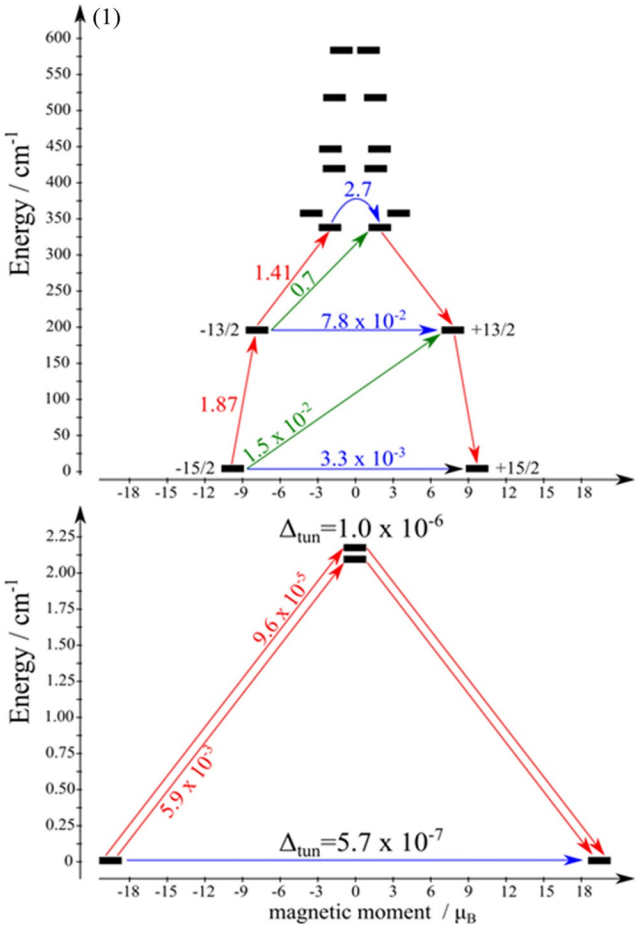

Figure 7. Top: Magnetization blocking barrier of Dy in Dy_2 (**1**). The thick black lines represent the KDs in accordance with the value of its magnetic moment. The green dashed lines correspond to diagonal QTM. The blue dashed lines represent Orbach relaxation processes; the red arrows show the most probable path for magnetic relaxation. The numbers at each arrow stand for the mean absolute value of the corresponding matrix element of the transition magnetic moment. Bottom: the low-lying exchange spectrum arising from the exchange interaction of the lowest KDs on the magnetic center (Δ_{tun} are corresponding tunneling gaps).

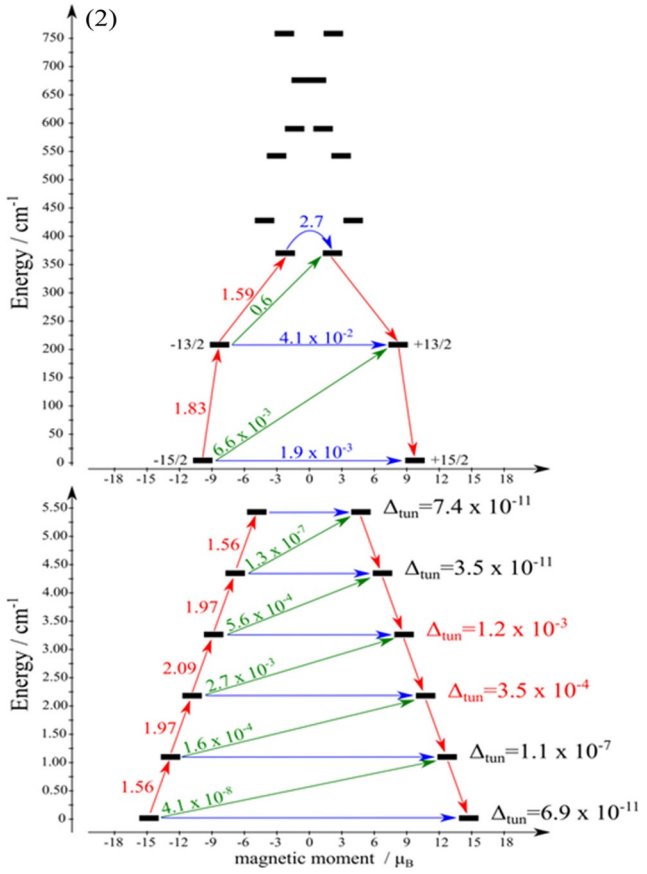

Figure 8. Top: magnetization blocking barrier of Dy in DyMn (**2**). The thick black lines represent the KDs in accordance with the value of its magnetic moment. The green dashed lines correspond to diagonal QTM; the blue dashed lines represent Orbach relaxation processes; the red arrows show the most probable path for magnetic relaxation. The numbers at each arrow stand for the mean absolute value of the corresponding matrix element of the transition magnetic moment. Bottom: the low-lying exchange spectrum arising from the exchange interaction of the lowest KDs on the magnetic center (Δ_{tun} are corresponding tunneling gaps).

splittings (10^{-4} and 10^{-3} cm^{-1} respectively), which thus open an important path for magnetic relaxation in this compound. We can associate this energy with the extracted exchange barrier of magnetic relaxation (3.7 cm^{-1}).

Conclusions

The particularly informative tailor-made pair of centrosymmetric dinuclear Dy_2 compound **1** and its heterometallic derivative DyMn **2** was developed to probe systematically the magnetic relaxation mechanism. Single-crystal X-ray diffraction showed that the molecular structures of **1** and **2** are priori comparable. Compound **1** shows typical SMM behavior with an energy gap Δ of 95.2 cm^{-1} and a pre-exponential factor τ_0 of 4.2×10^{-8} s in zero dc field, while no out-of-phase ac signal was observed for **2**. Through a detailed comparative study on these closely related model compounds, the structural and magnetic properties, especially the changes in the crystal-field splitting and anisotropy of the Dy site and the total exchange spectrum due to the replacement of Dy by Mn were investigated, and finally

Table 3. Exchange interactions between Dy^{III} ions in **1** and **2** obtained within the largest computational models employed. *zJ* is the parameter describing the intermolecular interaction. All values are given in cm^{-1}.

	Dy_2 (**1**)	DyMn (**2**)
$J_{total}^{*}=J_{exch}+J_{dipolar}$	0.185	0.454
J_{exch}	−0.023	0.330
$J_{dipolar}$[a]	0.208	0.124
zJ	−0.0024	−0.0146
J_{exch} from BS-DFT	−0.06	0.54

[a] Only J_{exch} was fitted to experimental data, while the value of the dipole–dipole interaction $J_{dipolar}$ is given here just for illustration, estimated as the difference $J_{total}^{*}-J_{exch}$. In practice, the dipole–dipole magnetic Hamiltonian was computed by using the ab initio results and added to the Lines exchange Hamiltonian. We mention here that this estimation of $J_{dipolar}$ was possible only because the dipole–dipole interaction is close to Ising type in these two particular cases, due to strong Ising anisotropy of the Dy sites in these compounds.

Table 4. The low-lying exchange spectrum [cm^{-1}] arising from the exchange interaction of the lowest Kramers doublets on magnetic centers in the compounds **1** and **2**.

Dy_2 (**1**)			DyMn (**2**)		
E	Δ_t	g_z	*E*	Δ_t	g_z
0.0000 0.0000	5.7377×10^{-7}	38.96	0.0000 0.0000	6.900×10^{-11}	29.54
2.1389 2.1389	1.0403×10^{-6}	0.00	1.0822 1.0822	1.1333×10^{-8}	25.56
191.9828 191.9828	3.6103×10^{-6}	35.56	2.1646 2.1649	3.5167×10^{-4}	21.59
192.1815 192.1815	2.8020×10^{-5}	35.56	3.2469 3.2481	1.2282×10^{-3}	17.63
193.4588 193.4588	1.9685×10^{-5}	0.00	4.3305 4.3305	3.5175×10^{-7}	13.69
193.5632 193.5632	1.5421×10^{-5}	0.00	5.4138 5.4138	7.4000×10^{-11}	9.81
334.2725 334.2740	1.5107×10^{-3}	27.30	204.6030 204.6030	4.2800×10^{-10}	26.56

the blocking barriers in these two compounds, which explain their different blocking behaviors, were rationalized. The Ising interaction in **1** suppresses the tunneling efficiently, and the magnetic relaxation at temperatures exceeding the exchange energy (2.14 cm^{-1}) must involve transition via the excited states, corresponding to local transitions in the excited doublet on the Dy site. In the case of **2**, the third and fourth exchange doublets at 2.16 and 3.25 cm^{-1}, respectively, show much larger tunneling splittings (10^{-4} and 10^{-3} cm^{-1} respectively), and thus an important path for magnetic relaxation in this compound is switched on.

This analysis was made possible by taking advantage of deliberate design of dinuclear model compounds with targeted metal replacement. Such a deep exploration enhances the understanding of magnetic interactions in elucidating the relaxation dynamics of lanthanide-containing systems and will then direct the rational design of new SMMs with high performance.

Experimental Section

General considerations

All reagents employed in the experiments were of analytical grade and used without further purification. The C, H, and N elemental analyses were performed with a PerkinElmer 2400 analyzer. The IR spectra were recorded with a VERTEX 70 FTIR spectrophotometer in the reflectance mode (4000–300 cm^{-1}); the samples were prepared as KBr disks.

X-ray crystallographic analysis and data collection

Crystallographic data and refinement details are given in Table 1. Suitable single crystals with dimensions of $0.30\times0.30\times0.20$, $0.30\times0.25\times0.21$, and $0.25\times0.25\times0.30$ mm for H_2opch, **1**, and **2**, respectively, were selected for single-crystal XRD. Crystallographic data were collected at 293 (H_2opch and **1**) and 273 K (**2**) on a Bruker ApexII CCD diffractometer with graphite-monochromated $Mo_{K\alpha}$ radiation ($\lambda = 0.71073$ Å). Data processing was accomplished with the SAINT processing program. The structure was solved by direct methods and refined on F^2 by full-matrix least-squares techniques with SHELXTL97.[34] All non-hydrogen atoms were refined with anisotropic thermal parameters. The H atoms were introduced in calculated positions and refined with fixed geometry with respect to their carrier atoms. CCDC 1030999 (H_2opch), 960070 (**1**) and 960071 (**2**) contain the supplementary crystallographic data for this paper. These data can be obtained free of charge from The Cambridge Crystallographic Data Centre.

Magnetic measurements

Magnetic susceptibility measurements were performed in the temperature range 2–300 K with a Quantum Design MPMS XL-7 SQUID magnetometer equipped with a 7 T magnet. The dc measurements were performed from 300 to 2 K and the ac measurements were carried out in a 3.0 Oe ac field oscillating at various frequencies from 1 to 1500 Hz. The diamagnetic corrections for the compounds were estimated by using Pascal's constants,[35] and magnetic data were corrected for diamagnetic contributions of the sample holder.

Computational methodology

Electronic and magnetic properties of individual metal centers in the Dy_2 and DyMn compounds were studied by fragment ab initio calculations with the MOLCAS-8.0 program package.[29] We employed the fragment approach because of the limitations of current ab initio methods and computers, which are not yet suitable to treat such binuclear complexes entirely ab initio. In this connection, the question arises how to build suitable mononuclear fragments from the molecules that would not change significantly the energy structure of the magnetic center. In order not to introduce additional errors, the full molecular structures of both molecules were employed. Since we aimed at directly comparing the calculated magnetism with that measured experimentally on crystalline samples, no geometry optimization of the fragments was done, and all atomic coordinates were taken from the X-ray analysis. Magnetic interaction was cancelled by substituting neighboring metal sites (containing unpaired electrons) by their diamagnetic equivalents. In **1**, the neighboring Dy^{III} ion was simulated by the closed-shell Lu^{III} ion, while in **2** the Mn^{II} site was simulated by the closed-shell Zn^{II} ion. In other words, a mononuclear Dy fragment is in fact the entire molecule in which all neighboring metal sites are substituted by their diamagnetic equivalents. All atoms were described by all-electron relativistic ANO-RCC basis sets available in the MOLCAS package.[36] Relativistic basis sets are suitable for the description of scalar relativistic effects by means of the Douglas–Kroll–Hess formalism.[37] These basis functions were used to optimize the electronic spin states of the individual metal sites within the active space of the complete active space self-consisting field (CASSCF) method.[38] The active space of the CASSCF calculation of the Dy included the 4f orbitals [CAS (9 in 7)], since we were interested in the ligand field states only. The 4f orbitals are well localized on the Ln site, which allows us to consider the metal-to-metal or metal-to-ligand charge-transfer states much higher in energy, and thus not relevant for the magnetism. The optimized spin states for ground and excited manifolds in CASSCF calculations were further mixed by the spin–orbit interaction in the restricted active space state interaction (RASSI) method.[37b,39] In this approach, the spin–orbit interaction is included by means of the atomic mean field approach (AMFI).[37b] Matrix elements of the orbital momentum over the spin states were also computed with the RASSI method. Ab initio calculated spectra and orbital momentum were further obtained by the SINGLE ANISO module[30] in MOLCAS to calculate the powder susceptibility, molar magnetization, and

the *g* tensors for the ground and several excited KDs of isolated metal fragments. In calculations of magnetic properties, all spin–orbit multiplets included within spin–orbit coupling in RASSI were taken into account. Therefore, including a large number of spin states in the spin–orbit mixing in the RASSI method is important for an accurate description of magnetism, in particular in cases of strong magnetic anisotropy.

For the simulation of magnetic properties of binuclear compounds we used an approach combining the calculated electronic and magnetic properties of individual metal fragments with the model description of the anisotropic exchange interaction between metal sites, achieved within the Lines model.[40] In this model, the isotropic Heisenberg exchange interaction is included between the true spins on neighboring metal sites ($\widehat{H}_{exch} = -J_{exch}\widehat{S}_1\widehat{S}_2$, where $S_{12}=5/2$ for Dy and Mn) in the absence of spin–orbit coupling. By considering explicitly (nonperturbatively) the spin–orbit interaction on the individual metal sites and expanding the interaction matrix in terms of the product of localized spin orbitals on individual metal sites, the resulting exchange matrix indeed describes the anisotropic exchange interaction. To this matrix we also added the dipolar–magnetic coupling between local magnetic moments. Diagonalization of the total interaction matrix (exchange + dipolar) provides the exchange (coupled) spectrum. These coupled eigenstates were further used to compute all measurable properties (magnetic susceptibility, molar magnetization, *g* tensors of the low-lying coupled eigenstates, etc.) of the entire binuclear systems in the POLY ANISO program.[30] The exchange parameters J_{ij} are usually extracted from the comparison between the calculated and measured magnetic data (magnetic susceptibility, molar magnetization) through minimization of the standard deviation, and are the only fitting parameters used in this approach. In the present case, this is just one fitting parameter describing the interaction between metal sites. Intermolecular interaction is accounted for in the mean-field approximation, by using one parameter describing the average exchange interaction between the considered molecule and neighboring ones (*zJ*).

An alternative approach to extract the exchange coupling constants employs BS-DFT calculations.[41] Since the orbitally near-degenerate ground state of the Dy^{III} sites complicates the DFT calculations, it must be replaced computationally by the closest atom with nondegenerate ground state. It was reported recently[13b] that BS calculations performed on the same molecular structure as initial compounds involving computational substitution of the Dy by Gd provide accurate values for the exchange couplings. In this approach, the exchange values obtained for the isostructural GdGd compound (two interacting spins of 7/2) must be rescaled for DyDy (two interacting spins of 5/2) by a factor of $7/5 \times 7/5 = 49/25$. For DyMn the rescaling involves only the spin of one metal site; therefore, the rescaling coefficient is 7/5.

Synthesis of H_2opch

Pyrazine-2-carboxylic acid methyl ester was prepared by a literature procedure described elsewhere.[15a] A mixture of pyrazine-2-carboxylic acid methyl ester (2.07 g, 15 mmol) and hydrazine hydrate (85%, 20 mL) in methanol (30 mL) was heated to reflux overnight at a temperature somewhat below 80 °C. The resulting pale yellow solution was set aside for 15 h. During this period, colorless pyrazine-2-carbohydrazide precipitated from the reaction mixture as a crystalline solid (yield: 1.35 g, 65%). Pyrazine-2-carbohydrazide (0.276 g, 2 mmol) was suspended together with *o*-vanillin (0.304 g, 2 mmol) in methanol (20 mL), and the resulting mixture was stirred at room temperature overnight. The pale yellow solid was collected by filtration. Then the product (0.054 g 0.2 mmol) was dissolved into CH_3OH/CH_2Cl_2 (25 mL, 1:1 v/v) to give a pale yellow solution. Pale yellow single crystals, suitable for X-ray diffraction analysis, were formed after 2 h (yield: 0.037 g, 68%). ^{1}H NMR (400 MHz, DMSO) $\delta = 12.62$ (s, 1H), 10.97 (s, 1H), 9.28 (d, $J = 1.6$ Hz, 1H), 8.94 (d, $J = 2.8$ Hz, 1H), 8.85 (s, 1H), 8.80–8.81 (m, 1H), 7.12 (dd, $J_1 = 1.2$ Hz, $J_2 = 8.0$ Hz, 1H), 7.05 (dd, $J_1 = 1.2$ Hz, $J_2 = 8.0$ Hz, 1H), 6.87 (t, $J = 8.0$ Hz, 1H), 3.82 (s, 3H); elemental analysis (%) calcd for $C_{13}H_{12}N_4O_3$: C 57.35, H 4.44, N 20.58: found C 57.64, H 4.59, N 20.39; IR (KBr): $\tilde{\nu} = 3415$(w), 3258(w), 1677(vs.), 1610(s), 1579(m). 1530(s), 1464(s), 1363(m), 1255(vs.), 1153(s), 1051(w), 1021(s), 986(w), 906(m), 938(w), 736(s), 596(m), 498 cm^{-1} (w).

Synthesis of $[Dy_2(opch)_2(OAc)_2(H_2O)_2]\cdot MeOH$ (1)

A solution of $Dy(OAc)_3\cdot 6H_2O$ (0.357 g, 0.1 mmol) and H_2opch (0.0405 g, 0.15 mmol) in CH_3OH/CH_2Cl_2 (20 mL, 1:1 v/v) was stirred with Et_3N (0.014 mL, 0.3 mmol) for 5 h. The resultant golden-yellow solution was left unperturbed to allow slow evaporation of the solvent. Golden-yellow single crystals, suitable for X-ray diffraction analysis, formed after one week. Yield: 18 mg (46% based on metal salt). Elemental analysis (%) calcd for $C_{32}H_{38}Dy_2N_8O_{14}$: C 35.47, H 3.53, N 10.34; found: C 34.96, H 3.41, N 10.42; IR (KBr): $\tilde{\nu} =$ 3389(br), 3057(w), 2841(w), 1607(vs.), 1561(m), 1519(w), 1478(s), 1465(w), 1454(s), 1417(m), 1381(m), 1341(w), 1303(m), 1285(w), 1245(m), 1216(s), 1159(m), 1087(w), 1031(w), 1019(w), 971(w) 872(w), 741(s), 644(w), 589(w), 431 cm^{-1} (m).

Synthesis of $[DyMn(opch)_2(OAc)(MeOH)(H_2O)_2]$ (2)

A solution of $Dy(OAc)_3\cdot 6H_2O$ (0.0357 mg, 0.1 mmol) and H_2opch (0.0405 mg, 0.15 mmol) in CH_3OH/CH_2Cl_2 (20 mL, 1:1 v/v) was stirred with Et_3N (0.014 mL, 0.3 mmol). After 3 h, $Mn(ClO_4)_2\cdot 6H_2O$ (36.2 mg, 0.1 mmol) was added to the solution. Then the mixture was stirred for a further 2 h, followed by filtration. The solution was left unperturbed to allow slow evaporation of the solvent. Dark red single crystals, suitable for X-ray diffraction analysis, were formed after three weeks. Yield: 24 mg (52%, based on $Dy(OAc)_3\cdot 6H_2O$). Elemental analysis (%) calcd for $C_{29}H_{32}DyMnN_8O_{11}$: C 39.31, H 3.64, N 12.65; found C 39.47, H 3.56, N 12.81; IR (KBr): $\tilde{\nu} =$ 3352(br), 3047(w), 2944(w), 2861(w), 1605(m), 1578(s), 1562(m), 1477(s), 1463(w), 1455(s), 1417(m), 1389(m), 1346(w), 1301(m), 1289(w), 1247(m), 1217(s), 1162(m), 1079(w), 1033(w), 972(w), 921(w), 869(w), 781(w), 739(s), 689(w), 665(w), 627(w), 587(w), 457(w), 429 cm^{-1} (m).

Acknowledgements

This work was supported by the National Natural Science Foundation of China (21525103, 21521092 and 21331003). J.T. gratefully acknowledges support of the Royal Society-Newton Advanced Fellowship (NA160075). L.U. is a post-doc of the Fonds Wetenschappelijk Onderzoek-Vlaanderen, and also gratefully acknowledges INPAC and Methusalem grants of K.U. Leuven. The computational resources and services used for the ab initio calculations were provided by the VSC (Flemish Supercomputer Center) and funded by the Hercules Foundation and the Flemish Government department EWI.

Conflict of interest

The authors declare no conflict of interest.

Keywords: ab initio calculations · lanthanides · magnetic properties · manganese · N,O ligands

[1] a) A. Caneschi, D. Gatteschi, R. Sessoli, A. L. Barra, L. C. Brunel, M. Guillot, *J. Am. Chem. Soc.* **1991**, *113*, 5873 – 5874; b) R. Sessoli, H. L. Tsai, A. R. Schake, S. Y. Wang, J. B. Vincent, K. Folting, D. Gatteschi, G. Christou, D. N. Hendrickson, *J. Am. Chem. Soc.* **1993**, *115*, 1804 – 1816; c) R. Sessoli, D. Gatteschi, A. Caneschi, M. A. Novak, *Nature* **1993**, *365*, 141 – 143.

[2] a) D. Gatteschi, R. Sessoli, J. Villain, *Molecular nanomagnets*, Oxford University Press, Oxford, **2006**; b) D. E. Freedman, W. H. Harman, T. D. Harris, G. J. Long, C. J. Chang, J. R. Long, *J. Am. Chem. Soc.* **2010**, *132*, 1224; c) M. N. Leuenberger, D. Loss, *Nature* **2001**, *410*, 789 – 793; d) S. Hill, R. S. Edwards, N. Aliaga-Alcalde, G. Christou, *Science* **2003**, *302*, 1015 – 1018; e) M. Mannini, F. Pineider, C. Danieli, F. Totti, L. Sorace, P. Sainctavit, M. A. Arrio, E. Otero, L. Joly, J. C. Cezar, A. Cornia, R. Sessoli, *Nature* **2010**, *468*, 417 – 421; f) M. L. Kahn, R. Ballou, P. Porcher, O. Kahn, J. P. Sutter, *Chem. Eur. J.* **2002**, *8*, 525 – 531; g) L. F. Chibotaru, L. Ungur, C. Aronica, H. Elmoll, G. Pilet, D. Luneau, *J. Am. Chem. Soc.* **2008**, *130*, 12445 – 12455; h) H. Oshio, M. Nihei, S. Koizumi, T. Shiga, H. Nojiri, M. Nakano, N. Shirakawa, M. Akatsu, *J. Am. Chem. Soc.* **2005**, *127*, 4568 – 4569; i) J. R. Friedman, M. P. Sarachik, J. Tejada, R. Ziolo, *Phys. Rev. Lett.* **1996**, *76*, 3830 – 3833; j) C. Aronica, G. Pilet, G. Chastanet, W. Wernsdorfer, J. F. Jacquot, D. Luneau, *Angew. Chem. Int. Ed.* **2006**, *45*, 4659 – 4662; *Angew. Chem.* **2006**, *118*, 4775 – 4778; k) R. Sessoli, A. K. Powell, *Coord. Chem. Rev.* **2009**, *253*, 2328 – 2341; l) M. A. AlDamen, J. M. Clemente-Juan, E. Coronado, C. Marti-Gastaldo, A. Gaita-Arino, *J. Am. Chem. Soc.* **2008**, *130*, 8874 – 8875; m) M. L. Kahn, J. P. Sutter, S. Golhen, P. Guionneau, L. Ouahab, O. Kahn, D. Chasseau, *J. Am. Chem. Soc.* **2000**, *122*, 3413 – 3421; n) G. Karotsis, S. Kennedy, S. J. Teat, C. M. Beavers, D. A. Fowler, J. J. Morales, M. Evangelisti, S. J. Dalgarno, E. K. Brechin, *J. Am. Chem. Soc.* **2010**, *132*, 12983 – 12990; o) V. Mereacre, Y. H. Lan, R. Clerac, A. M. Ako, I. J. Hewitt, W. Wernsdorfer, G. Buth, C. E. Anson, A. K. Rowell, *Inorg. Chem.* **2010**, *49*, 5293 – 5302.

[3] a) G. Christou, D. Gatteschi, D. N. Hendrickson, R. Sessoli, *MRS Bull.* **2000**, *25*, 66 – 71; b) J. M. Zadrozny, D. J. Xiao, M. Atanasov, G. J. Long, F. Grandjean, F. Neese, J. R. Long, *Nat. Chem.* **2013**, *5*, 577 – 581; c) C. M. Zaleski, E. C. Depperman, J. W. Kampf, M. L. Kirk, V. L. Pecoraro, *Angew. Chem. Int. Ed.* **2004**, *43*, 3912 – 3914; *Angew. Chem.* **2004**, *116*, 4002 – 4004; d) E. Coronado, P. Day, *Chem. Rev.* **2004**, *104*, 5419 – 5448; e) L. Bogani, W. Wernsdorfer, *Nat. Mater.* **2008**, *7*, 179 – 186; f) A. Dei, D. Gatteschi, *Angew. Chem. Int. Ed.* **2011**, *50*, 11852 – 11858; *Angew. Chem.* **2011**, *123*, 12054 – 12060; g) S. V. Eliseeva, J. C. G. Bunzli, *New J. Chem.* **2011**, *35*, 1165 – 1176; h) D. N. Woodruff, R. E. P. Winpenny, R. A. Layfield, *Chem. Rev.* **2013**, *113*, 5110 – 5148; i) D. Q. Wu, D. Shao, X. Q. Wei, F. X. Shen, L. Shi, D. Kempe, Y. Z. Zhang, K. R. Dunbar, X. Y. Wang, *J. Am. Chem. Soc.* **2017**, *139*, 11714 – 11717; j) J. K. Tang, I. Hewitt, N. T. Madhu, G. Chastanet, W. Wernsdorfer, C. E. Anson, C. Benelli, R. Sessoli, A. K. Powell, *Angew. Chem. Int. Ed.* **2006**, *45*, 1729 – 1733; *Angew. Chem.* **2006**, *118*, 1761 – 1765; k) S. G. McAdams, A. M. Ariciu, A. K. Kostopoulos, J. P. S. Walsh, F. Tuna, *Coord. Chem. Rev.* **2017**, *346*, 216 – 239; l) B. S. Dolinar, D. I. Alexandropoulos, K. R. Vignesh, T. James, K. R. Dunbar, *J. Am. Chem. Soc.* **2018**, *140*, 908 – 911; m) P. Abbasi, K. Quinn, D. I. Alexandropoulos, M. Damjanovic, W. Wernsdorfer, A. Escuer, J. Mayans, M. Pilkington, T. C. Stamatatos, *J. Am. Chem. Soc.* **2017**, *139*, 15644 – 15647.

[4] C. J. Milios, A. Vinslava, W. Wernsdorfer, S. Moggach, S. Parsons, S. P. Perlepes, G. Christou, E. K. Brechin, *J. Am. Chem. Soc.* **2007**, *129*, 2754.

[5] X. N. Yao, J. Z. Du, Y. Q. Zhang, X. B. Leng, M. W. Yang, S. D. Jiang, Z. X. Wang, Z. W. Ouyang, L. Deng, B. W. Wang, S. Gao, *J. Am. Chem. Soc.* **2017**, *139*, 373 – 380.

[6] N. Ishikawa, M. Sugita, T. Ishikawa, S. Koshihara, Y. Kaizu, *J. Am. Chem. Soc.* **2003**, *125*, 8694 – 8695.

[7] J. Liu, Y. C. Chen, J. L. Liu, V. Vieru, L. Ungur, J. H. Jia, L. F. Chibotaru, Y. H. Lan, W. Wernsdorfer, S. Gao, X. M. Chen, M. L. Tong, *J. Am. Chem. Soc.* **2016**, *138*, 5441 – 5450.

[8] Y. S. Ding, N. F. Chilton, R. E. P. Winpenny, Y. Z. Zheng, *Angew. Chem. Int. Ed.* **2016**, *55*, 16071 – 16074; *Angew. Chem.* **2016**, *128*, 16305 – 16308.

[9] a) F. S. Guo, B. M. Day, Y. C. Chen, M. L. Tong, A. Mansikkamaki, R. A. Layfield, *Angew. Chem. Int. Ed.* **2017**, *56*, 11445 – 11449; *Angew. Chem.* **2017**, *129*, 11603 – 11607; b) C. A. P. Goodwin, F. Ortu, D. Reta, N. F. Chilton, D. P. Mills, *Nature* **2017**, *548*, 439 – 442.

[10] Y. C. Chen, J. L. Liu, W. Wernsdorfer, D. Liu, L. F. Chibotaru, X. M. Chen, M. L. Tong, *Angew. Chem. Int. Ed.* **2017**, *56*, 4996 – 5000; *Angew. Chem.* **2017**, *129*, 5078 – 5082.

[11] J. D. Rinehart, M. Fang, W. J. Evans, J. R. Long, *J. Am. Chem. Soc.* **2011**, *133*, 14236 – 14239.

[12] a) F. Habib, M. Murugesu, *Chem. Soc. Rev.* **2013**, *42*, 3278 – 3288; b) F. Habib, P. H. Lin, J. Long, I. Korobkov, W. Wernsdorfer, M. Murugesu, *J. Am. Chem. Soc.* **2011**, *133*, 8830 – 8833; c) Y. N. Guo, G. F. Xu, W. Wernsdorfer, L. Ungur, Y. Guo, J. K. Tang, H. J. Zhang, L. F. Chibotaru, A. K. Powell, *J. Am. Chem. Soc.* **2011**, *133*, 11948 – 11951; d) P. Zhang, M. Perfetti, M. Kern, P. P. Hallmen, L. Ungur, S. Lenz, M. R. Ringenberg, W. Frey, H. Stoll, G. Rauhut, J. van Slageren, *Chem. Sci.* **2018**, *9*, 1221 – 1230; e) E. M. Pineda, N. F. Chilton, R. Marx, M. Dorfel, D. O. Sells, P. Neugebauer, S. D. Jiang, D. Collison, J. van Slageren, E. J. L. McInnes, R. E. P. Winpenny, *Nat. Commun.* **2014**, *5*, 5243; f) R. A. Layfield, J. J. W. McDouall, S. A. Sulway, F. Tuna, D. Collison, R. E. P. Winpenny, *Chem. Eur. J.* **2010**, *16*, 4442 – 4446; g) F. Habib, G. Brunet, V. Vieru, I. Korobkov, L. F. Chibotaru, M. Murugesu, *J. Am. Chem. Soc.* **2013**, *135*, 13242 – 13245.

[13] a) K. C. Mondal, A. Sundt, Y. H. Lan, G. E. Kostakis, O. Waldmann, L. Ungur, L. F. Chibotaru, C. E. Anson, A. K. Powell, *Angew. Chem. Int. Ed.* **2012**, *51*, 7550 – 7554; *Angew. Chem.* **2012**, *124*, 7668 – 7672; b) S. K. Langley, D. P. Wielechowski, V. Vieru, N. F. Chilton, B. Moubaraki, B. F. Abrahams, L. F. Chibotaru, K. S. Murray, *Angew. Chem. Int. Ed.* **2013**, *52*, 12014 – 12019; *Angew. Chem.* **2013**, *125*, 12236 – 12241; c) S. K. Langley, D. P. Wielechowski, V. Vieru, N. F. Chilton, B. Moubaraki, L. F. Chibotaru, K. S. Murray, *Chem. Commun.* **2015**, *51*, 2044 – 2047; d) A. Upadhyay, C. Das, S. Vaidya, S. K. Singh, T. Gupta, R. Mondol, S. K. Langley, K. S. Murray, G. Rajaraman, M. Shanmugam, *Chem. Eur. J.* **2017**, *23*, 4903 – 4916.

[14] H. Q. Tian, L. Zhao, H. F. Lin, J. K. Tang, G. S. Li, *Chem. Eur. J.* **2013**, *19*, 13235 – 13241.

[15] a) H. Q. Tian, L. Zhao, Y. N. Guo, Y. Guo, J. K. Tang, Z. L. Liu, *Chem. Commun.* **2012**, *48*, 708 – 710; b) H. Q. Tian, M. Wang, L. Zhao, Y. N. Guo, Y. Guo, J. K. Tang, Z. L. Liu, *Chem. Eur. J.* **2012**, *18*, 442 – 445.

[16] R. A. Coxall, S. G. Harris, D. K. Henderson, S. Parsons, P. A. Tasker, R. E. P. Winpenny, *J. Chem. Soc. Dalton* **2000**, 2349 – 2356.

[17] S. R. Batten, S. M. Neville, D. R. Turner, *Coord. Polym. Des. Anal. Appl.* **2009**, 19 – 58.

[18] D. Casanova, M. Llunell, P. Alemany, S. Alvarez, *Chem. Eur. J.* **2005**, *11*, 1479 – 1494.

[19] O. Kahn, *Molecular magnetism*, Wiley, New York, **1993**.

[20] a) I. J. Hewitt, Y. H. Lan, C. E. Anson, J. Luzon, R. Sessoli, A. K. Powell, *Chem. Commun.* **2009**, 6765 – 6767; b) K. Katoh, T. Kajiwara, M. Nakano, Y. Nakazawa, W. Wernsdorfer, N. Ishikawa, B. K. Breedlove, M. Yamashita, *Chem. Eur. J.* **2011**, *17*, 117 – 122; c) B. Hussain, D. Savard, T. J. Burchell, W. Wernsdorfer, M. Murugesu, *Chem. Commun.* **2009**, 1100 – 1102.

[21] a) V. Mereacre, M. N. Akhtar, Y. H. Lan, A. M. Ako, R. Clerac, C. E. Anson, A. K. Powell, *Dalton Trans.* **2010**, *39*, 4918 – 4927; b) C. M. Liu, D. Q. Zhang, D. B. Zhu, *Dalton Trans.* **2010**, *39*, 11325 – 11328; c) S. K. Langley, B. Moubaraki, K. S. Murray, *Dalton Trans.* **2010**, *39*, 5066 – 5069; d) C. M. Zaleski, J. W. Kampf, T. Mallah, M. L. Kirk, V. L. Pecoraro, *Inorg. Chem.* **2007**, *46*, 1954 – 1956.

[22] V. Mereacre, A. M. Ako, R. Clerac, W. Wernsdorfer, I. J. Hewitt, C. E. Anson, A. K. Powell, *Chem. Eur. J.* **2008**, *14*, 3577 – 3584.

[23] N. F. Chilton, S. K. Langley, B. Moubaraki, K. S. Murray, *Chem. Commun.* **2010**, *46*, 7787 – 7789.

[24] a) A. H. Cooke, C. B. P. Finn, B. W. Mangum, R. L. Orbach, *J. Phys. Soc. Jpn.* **1962**, *17*, 462; b) C. B. Finn, R. Orbach, W. P. Wolf, *Proc. Phys. Soc. London* **1961**, *77*, 261.

[25] a) S. Nayak, O. Roubeau, S. J. Teat, C. M. Beavers, P. Gamez, J. Reedijk, *Inorg. Chem.* **2010**, *49*, 216 – 221; b) A. Okazawa, T. Nogami, H. Nojiri, T. Ishida, *Chem. Mater.* **2008**, *20*, 3110 – 3119.

[26] a) M. Ferbinteanu, T. Kajiwara, K. Y. Choi, H. Nojiri, A. Nakamoto, N. Kojima, F. Cimpoesu, Y. Fujimura, S. Takaishi, M. Yamashita, *J. Am. Chem. Soc.* **2006**, *128*, 9008 – 9009; b) V. Chandrasekhar, B. M. Pandian, R. Boo-

mishankar, A. Steiner, J. J. Vittal, A. Houri, R. Clerac, *Inorg. Chem.* **2008**, *47*, 4918 – 4929.
[27] A. Bhunia, M. T. Gamer, L. Ungur, L. F. Chibotaru, A. K. Powell, Y. H. Lan, P. W. Roesky, F. Menges, C. Riehn, G. Niedner-Schatteburg, *Inorg. Chem.* **2012**, *51*, 9589 – 9597.
[28] a) L. Ungur, W. Van den Heuvel, L. F. Chibotaru, *New J. Chem.* **2009**, *33*, 1224 – 1230; b) D. Visinescu, A. M. Madalan, M. Andruh, C. Duhayon, J. P. Sutter, L. Ungur, W. Van den Heuvel, L. F. Chibotaru, *Chem. Eur. J.* **2009**, *15*, 11808 – 11814.
[29] F. Aquilante, J. Autschbach, R. K. Carlson, L. F. Chibotaru, M. G. Delcey, L. De Vico, I. F. Galvan, N. Ferre, L. M. Frutos, L. Gagliardi, M. Garavelli, A. Giussani, C. E. Hoyer, G. Li Manni, H. Lischka, D. X. Ma, P. A. Malmqvist, T. Muller, A. Nenov, M. Olivucci, T. B. Pedersen, D. L. Peng, F. Plasser, B. Pritchard, M. Reiher, I. Rivalta, I. Schapiro, J. Segarra-Marti, M. Stenrup, D. G. Truhlar, L. Ungur, A. Valentini, S. Vancoillie, V. Veryazov, V. P. Vysotskiy, O. Weingart, F. Zapata, R. Lindh, *J. Comput. Chem.* **2016**, *37*, 506 – 541.
[30] L. Ungur, L. F. Chibotaru, University of Leuven, **2006** – **2017**.
[31] F. Neese, *Wires Comput. Mol. Sci.* **2012**, *2*, 73 – 78.
[32] D. A. Pantazis, F. Neese, *J. Chem. Theory Comput.* **2009**, *5*, 2229 – 2238.
[33] L. Gagliardi, R. Lindh, G. Karlstrom, *J. Chem. Phys.* **2004**, *121*, 4494 – 4500.
[34] G. M. Sheldrick, *Acta Crystallogr. Sect. A* **2008**, *64*, 112 – 122.
[35] G. A. Bain, J. F. Berry, *J. Chem. Educ.* **2008**, *85*, 532 – 536.
[36] a) B. O. Roos, R. Lindh, P. A. Malmqvist, V. Veryazov, P. O. Widmark, *J. Phys. Chem. A* **2004**, *108*, 2851 – 2858; b) B. O. Roos, R. Lindh, P. A. Malmqvist, V. Veryazov, P. O. Widmark, *J. Phys. Chem. A* **2005**, *109*, 6575 – 6579; c) B. O. Roos, R. Lindh, P. A. Malmqvist, V. Veryazov, P. O. Widmark, A. C. Borin, *J. Phys. Chem. A* **2008**, *112*, 11431 – 11435.
[37] a) M. Douglas, N. M. Kroll, *Ann. Phys.* **1974**, *82*, 89 – 155; b) B. A. Hess, C. M. Marian, U. Wahlgren, O. Gropen, *Chem. Phys. Lett.* **1996**, *251*, 365 – 371; c) M. Reiher, *Wires Comput. Mol. Sci.* **2012**, *2*, 139 – 149.
[38] a) B. O. Roos, *Int. J. Quantum. Chem.* **1980**, *17*, 175 – 189; b) B. O. Roos, P. R. Taylor, P. E. M. Siegbahn, *Chem. Phys.* **1980**, *48*, 157 – 173; c) P. E. M. Siegbahn, J. Almlof, A. Heiberg, B. O. Roos, *J. Chem. Phys.* **1981**, *74*, 2384 – 2396.
[39] a) P. A. Malmqvist, B. O. Roos, *Chem. Phys. Lett.* **1989**, *155*, 189 – 194; b) P. A. Malmqvist, B. O. Roos, B. Schimmelpfennig, *Chem. Phys. Lett.* **2002**, *357*, 230 – 240.
[40] M. E. Lines, *J. Chem. Phys.* **1971**, *55*, 2977.
[41] a) E. Ruiz, P. Alemany, S. Alvarez, J. Cano, *J. Am. Chem. Soc.* **1997**, *119*, 1297 – 1303; b) E. Ruiz, J. Cano, S. Alvarez, P. Alemany, *J. Comput. Chem.* **1999**, *20*, 1391 – 1400; c) P. J. Hay, J. C. Thibeault, R. Hoffmann, *J. Am. Chem. Soc.* **1975**, *97*, 4884 – 4899; d) M. Shoji, K. Koizumi, Y. Kitagawa, T. Kawakami, S. Yamanaka, M. Okumura, K. Yamaguchi, *Chem. Phys. Lett.* **2006**, *432*, 343 – 347.

Manuscript received: March 27, 2018
Accepted manuscript online: April 26, 2018
Version of record online: June 25, 2018